GEOLOGY | THE GEOLOGICAL SOCIETY OF AMERICA®

https://doi.org/10.1130/G45526.1

Manuscript received 27 August 2018
Revised manuscript received 28 November 2018
Manuscript accepted 10 December 2018

Published online 8 January 2019

First identification of postcollisional A-type magmatism in the Himalayan-Tibetan orogen

Lu-Lu Hao[1,2], Qiang Wang[1,3,4]*, Derek A. Wyman[5], Lin Ma[1], Jun Wang[1], Xiao-Ping Xia[1], and Quan Ou[1]

[1]State Key Laboratory of Isotope Geochemistry, Guangzhou Institute of Geochemistry, Chinese Academy of Sciences (CAS), Guangzhou 510640, China

[2]CAS Key Laboratory of Crust-Mantle Materials and Environments, School of Earth and Space Sciences, University of Science and Technology of China, Hefei 230026, China

[3]CAS Center for Excellence in Tibetan Plateau Earth Sciences, Beijing 100101, China

[4]College of Earth and Planetary Sciences, University of Chinese Academy of Sciences, Beijing 10049, China

[5]School of Geosciences, The University of Sydney, Sydney, NSW 2006, Australia

ABSTRACT

A-type magmatism is commonly generated in extensional settings. Cenozoic postcollisional extensional structures and magmatism widely occur in the well-known Himalayan-Tibetan orogen (HTO). So far, however, no Cenozoic A-type magmatism has been identified in the orogen. Here, we report on newly identified 24–23 Ma felsic lavas (trachytes + rhyolites) in the Konglong area of the Lhasa block, southern Tibet. They have diagnostic minerals (sodalites) and geochemical characteristics (high total-alkali, FeO/MgO, Zr, and Ga/Al, low CaO, and strongly negative Eu, Sr, and Ba anomalies), demonstrating their close affinity with A-type granitoids. Generation of the A-type lavas required high-temperature melting (up to 944 °C) of crustal source rocks in the pressure range of 0.5–1.2 GPa. Our study not only identifies the first postcollisional A-type magmatism in the HTO, but it also indicates an extension event contemporaneous with the onset of the Main Central thrust and South Tibetan detachment system, and development of the Kailas basin and ultrapotassic magmatism of the southern HTO. These events straddled the Himalaya and Lhasa blocks and can be reconciled with foundering of the subducted Indian plate. Thus, we suggest a tectonic model of Indian plate flat subduction and foundering beneath the western Lhasa block for the postcollisional evolution of the southern HTO.

INTRODUCTION

A-type granitoids are chemically characterized by high total-alkali, Zr, and Ga contents; and low CaO, Ba, Eu, and Sr contents; and high FeO/MgO and Ga/Al values (Whalen et al., 1987). They vary in composition from syenites to granites and their respective volcanic equivalents (SiO_2 = 55–80 wt%; Eby, 1992). A-type granitoids crystallize from relatively high-temperature magmas and occur in extensional (rift, plume or hotspot, or postcollisional) settings (Eby, 1992).

The Himalayan-Tibetan orogen (HTO), one of the most prominent continent-continent collision zones in the Cenozoic, resulted from India-Asia collision and convergence (Yin and Harrison, 2000). Postcollisional extensional structures and magmatism widely occur in the orogen, but no Cenozoic A-type magmatism has been reported (Yin and Harrison, 2000; DeCelles et al., 2002; Chung et al., 2005). Recently, we identified a new type of felsic lava in the Konglong area of the Lhasa block (LB). Our data show that these lavas formed at 24–23 Ma and are similar to typical A-type granitoids. This is the first postcollisional A-type magmatism identified in the HTO and indicates late Oligocene–early Miocene extension of the LB. Combined with contemporaneous geological events, we propose a modified geodynamic model for the Cenozoic evolution of the southern HTO.

GEOLOGICAL SETTING AND SAMPLES

The HTO consists primarily of the Songpan-Ganze, Qiangtang, Lhasa, and Himalaya blocks (Fig. 1; Yin and Harrison, 2000). Lhasa-India collision and convergence built the HTO, but the detailed tectonic evolution remains debated. Here, we briefly review the postcollisional tectonics and magmatism in the southern HTO (see the review of DeCelles et al., 2002).

Most structures in the southern Himalaya are contractional and record north-south crustal shortening and include the Main Central thrust, the Main Boundary thrust, and the Main Frontier thrust. The northern Himalaya is characterized by extensional structures (e.g., the east-west–trending South Tibetan detachment system [STDS], north Himalayan gneiss domes, and north-south–trending rifts). The onset of the STDS and Main Central thrust is widely considered to have been near-synchronous (24–23 Ma; DeCelles et al., 2002).

The major thrusts accommodating crustal shortening in the LB were active between the Late Cretaceous and 25 Ma (Wang et al., 2014). The north-south–trending extensional structures are the most distinct features of the LB, and their initiation is constrained by the 18 Ma Pabaizong dikes (Williams et al., 2001). In addition, the east-west–trending Kailas basin developed along the Indus-Zangpo suture beginning in the late Oligocene (26–24 Ma; DeCelles et al., 2011).

Postcollisional magmatism in the Himalaya consists of 46–26 Ma adakitic granites and 26–7 Ma leucogranites, which were generally linked to crustal thickening and extension, respectively (Wu et al., 2015). Postcollisional magmatism in the LB is composed of 25–8 Ma potassic-ultrapotassic and 38–10 Ma adakitic rocks (Fig. 1). The ultrapotassic magmas are widely interpreted to have originated from a mantle source enriched by the subducted Indian plate (Zhao et al., 2009; Guo et al., 2015).

*E-mail: wqiang@gig.ac.cn

CITATION: Hao, L.-L., et al., 2019, First identification of postcollisional A-type magmatism in the Himalayan-Tibetan orogen: Geology, v. 47, p. 187–190, https://doi.org/10.1130/G45526.1.

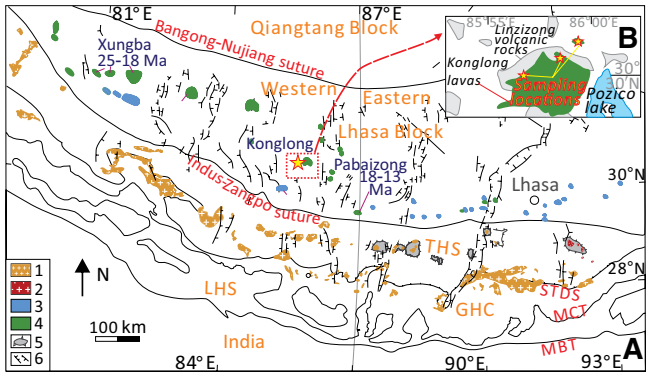

Figure 1. A: Geological map showing main tectonics and Cenozoic magmatism of southern Himalayan-Tibetan orogen (HTO), modified after Zheng et al. (2016). STDS—South Tibetan detachment system; MCT—Main Central thrust; MBT—Main Boundary thrust; THS—Tethyan Himalayan Sequence; GHC—Greater Himalayan crystalline complex; LHS—Lesser Himalayan Sequence. Legend: (1,2) 44–7 Ma leucogranite and 46–35 Ma adakite of Himalaya, respectively; (3,4) 38–10 Ma adakite and 25–8 Ma (ultra)potassic rock of Lhasa, respectively; (5) northern Himalayan gneiss dome; (6) north-south normal fault. B: Simplified map showing volcanism in Konglong area.

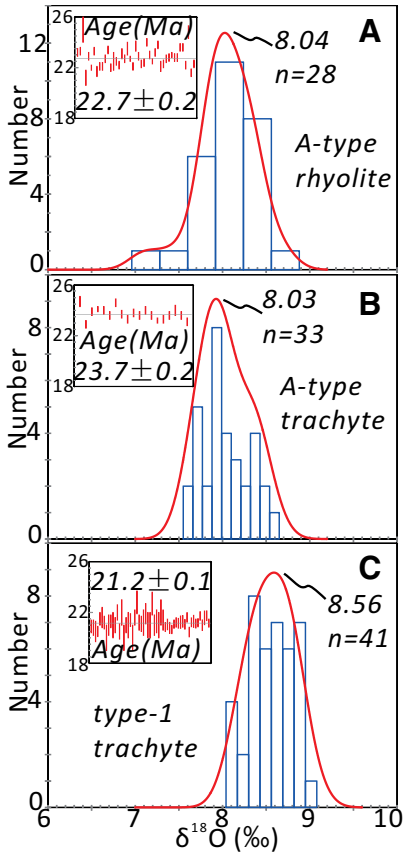

Figure 2. Zircon U-Pb ages and O isotopes for Konglong (southern Tibet) lavas.

Chen et al. (2010) studied the 21 Ma potassic lavas (referred to here as "type-1" trachytes-rhyolites) in the Konglong area of the LB. Here, we revisited the Konglong lavas, where a new type of lava (type-2) was found on the northern and western margins (Fig. 1).

RESULTS

The Konglong type-2 trachytes have rare mafic minerals, and the phenocrysts consist mainly of K-feldspar (Kfs) with minor plagioclase (Pl; Figs. DR2a–DR2c in the GSA Data Repository[1]). Some phenocryst sodalites are also observed (Fig. DR2a). In contrast, the type-1 trachytes have abundant mafic minerals (clinopyroxene [Cpx], amphibole [Amp], phlogopite [Phl]) and Kfs with minor Pl and quartz (Qz) as phenocrysts but no sodalite (Figs. DR2g–DR2i). Phenocrysts in the type-2 rhyolites consist of Pl, Kfs, and Qz (Figs. DR2d–DR2f).

The type-2 rhyolites and trachytes have laser ablation–inductively coupled plasma–mass spectrometry (LA-ICP-MS) zircon U-Pb ages of 22.7 ± 0.2 Ma and 23.7 ± 0.2 Ma, respectively (Figs. 2A and 2B). No inherited zircons or cores have been found (Fig. DR3). Their zircons show similar $\delta^{18}O$ ranges of 7.1‰–8.7‰ and 7.6‰–8.6‰, with average values of 8.04‰ and 8.03‰, respectively (Figs. 2A and 2B). In contrast, the type-1 trachytes have a zircon age of 21.2 ± 0.1 Ma and $\delta^{18}O$ ranges of 8.1‰–9.1‰, with an average value of 8.56‰ (Fig. 2C).

The type-2 lavas have high SiO_2 (63–77 wt%), $K_2O + Na_2O$ (9.1–13.6 wt%; Fig. 3A), and K_2O (5.3–8.3 wt%), and low MgO (0.06–0.10 wt%) and CaO (0.3–1.5 wt%). Accordingly, they have high FeO/(FeO + MgO) values (0.88–0.98) and $(K_2O + Na_2O)$/CaO (9–33) values (Figs. 3B and 3C). The type-2 trachytes and rhyolites show parallel trace-element distribution patterns that are characterized by significant light rare earth element (LREE) fractionation with La/Sm_N = 12–23, heavy REE (HREE) depletion with La/Yb_N = 61–81, and strongly negative Ba, Sr, and Eu anomalies, which are similar to those of typical A-type granitoids (Fig. 3D; Eby, 1992).

The type-2 lavas show enriched Sr-Nd isotopic signatures, i.e., high $(^{87}Sr/^{86}Sr)_i$ of 0.709–0.711 and low $\varepsilon_{Nd(t)}$ of –10.4 to –9.7, which are slightly less enriched than those of type-1 lavas (Fig. 3E; Chen et al., 2010).

DISCUSSION

First Postcollisional A-Type Magmatism in the HTO

Our zircon U-Pb ages for the Konglong lavas and a whole-rock ^{40}Ar-^{39}Ar age of a type-1 rhyolite (21.3 ± 0.2 Ma; Chen et al., 2010) suggest that the type-2 lavas formed at 24–23 Ma, slightly earlier than type-1 lavas (21 Ma).

The type-2 lavas show different mineral assemblages and major- and trace-element characteristics from the type-1 lavas and widespread potassic-ultrapotassic lavas, adakites, leucogranites, and peraluminous rhyolites of the HTO. First, while the type-2 and type-1 lavas show similar SiO_2 ranges, they define distinct major-element compositional trends (Fig. DR4). Second, the type-2 lavas have no mafic phenocrysts and show strong LREE fractionation. In contrast, the type-1 and potassic-ultrapotassic lavas generally contain abundant phenocrysts of Phl and Cpx and/or Amp and show low La/Sm_N (<8). Third, the type-2 lavas have high SiO_2, low MgO, and variable K_2O/Na_2O (1–1.5; except for one high-SiO_2 sample with K_2O/Na_2O = 5.9), clearly deviating from the field of Lhasa ultrapotassic lavas (Fig. 3A). Fourth, the type-2 lavas show strongly negative Eu and Sr anomalies and low Sr/Y and thus are distinct from adakites (Fig. 3F). Finally, the type-2 lavas differ from the leucogranites and peraluminous rhyolites (Fig. DR5) by low A/CNK [molar $Al_2O_3/(CaO + Na_2O + K_2O)$ = 0.90–1.07], high Zr contents (202–1537 ppm), and absence of muscovite, tourmaline, or garnet. Leucogranites and peraluminous rhyolites mainly show high A/CNK (>1.0) and low Zr contents (<200 ppm). No other Cenozoic magmatic rocks with the distinct mineralogical and geochemical features of the Konglong type-2 lavas have ever been reported in the HTO.

Globally, the diagnostic minerals (e.g., sodalite phenocrysts) and geochemical features (Figs. 3A–3D) of the Konglong type-2 lavas indicate their close affinity with A-type granitoids (Eby, 1992). On discrimination diagrams for A-type granitoids (Figs. 3B and 3C), they are readily distinguished from potassic-ultrapotassic lavas and adakites and exclusively plot in the A-type field. Their strongly negative Eu, Sr, and Ba anomalies and high Zr contents and zircon saturation temperatures (T_{Zr} = 775–944 °C; Fig. DR5) are also completely consistent with those of A-type granitoids. Therefore, the 24–23 Ma Konglong lavas in the LB represent the first postcollisional A-type magmatism found in the HTO.

Genesis of A-Type Lavas

Mechanisms involving melting of crustal sources, crust- and mantle-derived magma mixing, or fractional crystallization, with/without crustal assimilation (A) of mantle-derived magmas, are often suggested to explain the origin of

[1]GSA Data Repository item 2019066, analytical methods and data, and Figures DR1–DR6, is available online at http://www.geosociety.org/datarepository/2019/, or on request from editing@geosociety.org.

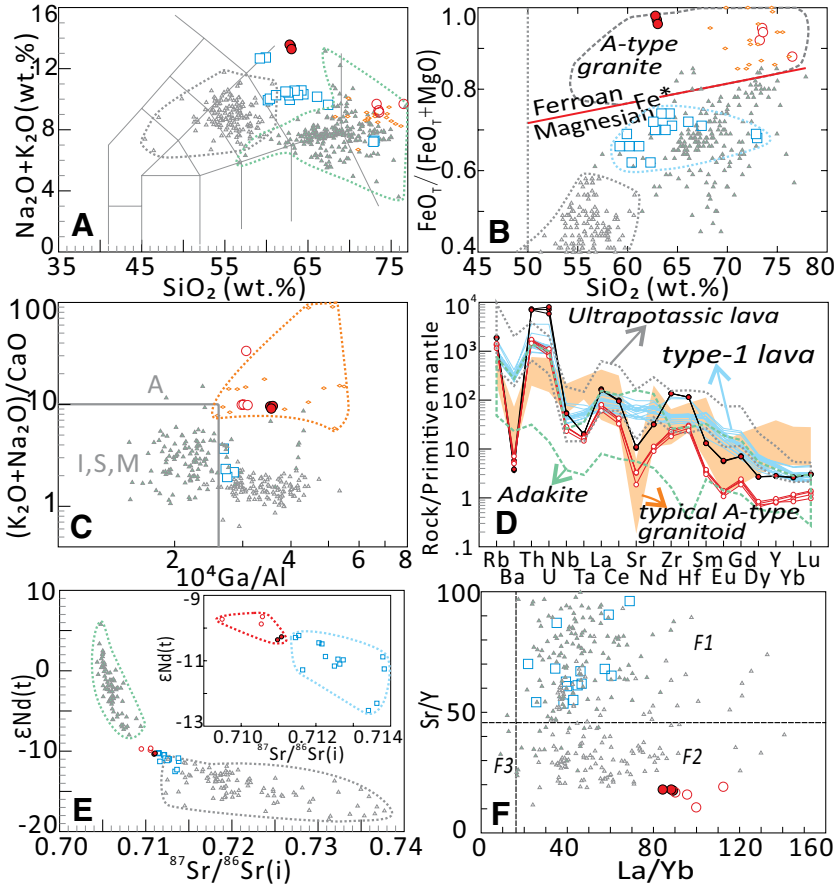

Figure 3. Geochemical diagrams for Konglong (southern Tibet) A-type lavas. A: SiO_2 versus (K_2O + Na_2O). B: SiO_2 versus FeO_T/(FeO_T + MgO) (Frost et al., 2001). C: Ga/Al versus (K_2O + Na_2O)/CaO (Whalen et al., 1987). D: Trace-element distribution pattern. E: Sr-Nd isotopes. F: La/Yb vs. Sr/Y (Wang et al., 2016). F1–F3 are crustal melts in the stability fields of garnet (Grt) with little or no plagioclase (Pl), with Pl and Grt, and Pl with little or no Grt, respectively. Closed and open circles are A-type trachytes and rhyolites, respectively; open squares are type-1 lavas; open and closed triangles are ultrapotassic and adakitic rocks, respectively.

A-type magmas (Eby, 1992). Here, we suggest that the first model can account well for the Konglong A-type trachytes.

First, the high SiO_2 and low MgO values of A-type trachytes suggest that they were not directly derived from the upper mantle. Second, they could not be produced by fractional crystallization of coeval ultrapotassic magmas because they have lower REE contents and clearly distinct trace-element distribution patterns (Fig. 3D). Third, the A-type trachytes formed at very high temperatures (up to 944 °C), suggesting that extensive (A) fractional crystallization from ultrapotassic magmas was not feasible. Furthermore, the Konglong type-1 trachytes and rhyolites were considered to have originated from the Lhasa lower and middle-upper crust, respectively (Chen et al., 2010). However, both of these crust-derived rocks and ultrapotassic lavas have more enriched Sr-Nd isotopic compositions and higher Sr/Y than the A-type trachytes (Figs. 3E and 3F), suggesting the latter cannot be produced by mixing of crustal and ultrapotassic magmas. Finally, the high SiO_2, low MgO, and enriched Sr-Nd-O isotopes of the A-type trachytes support a crustal origin. Compared to type-1 lavas, the A-type trachytes show slightly less enriched Sr-Nd-O isotope compositions (Figs. 2 and 3E), suggesting the involvement of some juvenile materials in their sources. The mineral assemblages in crustal source rocks of the A-type trachytes can be constrained by their geochemical features. The distinctly negative Sr and Eu anomalies, high-La/Yb, and low-Sr/Y values of A-type trachytes (Fig. 3F) likely reflect the presence of residual Pl and Grt in their sources. Therefore, given that the lower limit of garnet (Grt) stability is 0.5 GPa, and Pl will disappear at pressures >1.2–1.5 GPa (Rapp et al., 2003; Wang et al., 2016), the Konglong A-type trachytes were likely generated by high-temperature melting (up to 944 °C) of crustal source rocks (ancient + juvenile materials) in the pressure range of 0.5–1.2 GPa.

The A-type rhyolites have extremely similar trace-element distribution patterns and Sr-Nd and zircon oxygen isotope compositions to the A-type trachytes, indicating a close genetic link. Their very low REE contents could likely indicate that fractionation of REE-enriched accessory minerals (e.g., titanite) played a key role during their generation.

GEODYNAMIC IMPLICATIONS

Numerous studies have suggested that the India-Lhasa (Eurasia) initial collision occurred during the early Cenozoic, which eventually induced oceanic slab breakoff at 50–45 Ma (DeCelles et al., 2011), after which the collision zone converted into a postcollisional intracontinental setting with northward underthrusting of the Indian plate beneath the LB. However, the detailed tectonic process of Indian plate subduction remains controversial (DeCelles et al., 2011; Chung et al., 2005).

Segmentation of the subducted Indian plate (Wang et al., 2018) appears likely because geophysical data have recently shown that the northward subduction angle of the Indian plate beneath the LB increases from west to east (Chen et al., 2015). Indian plate steep subduction for a short distance beneath the eastern LB (ELB; east of longitude 87°E) is consistent with the spatial distribution of the ELB postcollisional adakitic magmatism (Hou et al., 2012), which was restricted to the ELB southern margin (Fig. 1). As for the western LB (WLB; west of 87°E), a clear magmatic gap between 45 and 25 Ma is consistent with Indian plate flat subduction. In addition, the mantle source of the ≤25 Ma ultrapotassic lavas has widely been suggested to include Indian components, indicating that the Indian plate must have subducted at a low angle and reached beneath the central-northern WLB no later than 25 Ma (Hao et al., 2018).

Renewed WLB magmatism after the 45–25 Ma magmatic gap consists of 25–8 Ma potassic-ultrapotassic lavas. The tectonic setting for this magmatism remains debated. Previous studies suggested an east-west extensional setting for these lavas, mainly based on their close association with north-south–trending rifts (Zhao et al., 2009). However, the discrepancy between the onset of this magmatism (25 Ma) and north-south–trending rifts (18 Ma; Williams et al., 2001) could argue against this suggestion. The onset of this magmatism, instead, was nearly coeval with the development (26–24 Ma) of the Kailas basin (DeCelles et al., 2011), which suggests a likely genetic link to north-south extension. However, no direct link between the deep mantle process generating this renewed magmatism and crustal extension has previously been observed.

Our study on the 24–23 Ma Konglong A-type magmatism indicates a crustal high-temperature melting event within an extensional setting that was nearly coeval with the onset of the ultrapotassic magmatism and Kailas basin formation. Given the magmatic gap and inferred Indian plate flat subduction and the WLB cold crust during 45–25 Ma, the crustal high-temperature melting responsible for the Konglong A-type

magmatism likely reflects a thermal transformation related to a deep mantle process. Accordingly, the crustal melting and N-S extension were probably linked to foundering of Asian lithosphere (Chung et al., 2005) or Indian plate rollback and breakoff (DeCelles et al., 2011).

In addition, the Konglong A-type magmatism, Kailas basin, and potassic-ultrapotassic magmatism of the WLB were coeval with the extrusion of the Greater Himalayan crystalline complex (i.e., the onset of the Main Central thrust to the south and STDS to the north) of the Himalaya (DeCelles et al., 2002). These diverse events straddled both the Himalaya and Lhasa blocks, but their distribution and common timing can be reconciled if they were related to foundering of the northward subducted Indian plate (DeCelles et al., 2002, 2011). This scenario is consistent with recent geophysical data (Chen et al., 2017) that indicate a T-shaped high-wave-speed structure beneath the southern HTO, inferred to be a remnant from earlier plate foundering. We do not stress Indian plate rollback because no southward migration of the WLB postcollisional magmatism was observed (Fig. 1).

Integrating the observations above, we propose a modified tectonic model for the Cenozoic evolution of the Himalaya-WLB orogen (Fig. 4; Fig. DR6) that provides an internally consistent explanation for all of these geological events:

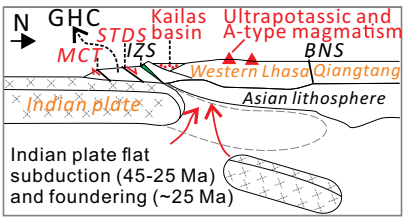

Figure 4. Simple cartoon showing 25–24 Ma geodynamics of Himalaya–western Lhasa orogen, modified from DeCelles et al. (2011). Detailed tectonic evolution is presented in Figure DR6 (see text footnote 1). STDS—South Tibetan detachment system; MCT—Main Central thrust; GHC—Greater Himalayan crystalline complex; IZS—Indus-Zangpo suture; BNS—Bangong-Nujiang suture.

(1) Following the Neo-Tethyan oceanic slab breakoff at 50–45 Ma, Indian plate flat subduction beneath the WLB occurred during 45–25 Ma, which caused the WLB magmatic gap. In this stage, crustal thickening of the underthrusting Indian plate contributed to the Eocene–Oligocene (46–26 Ma) magmatism in the Himalaya (Fig. 1; Hou et al., 2012).

(2) After ca. 25 Ma, foundering of the flat Indian plate caused significant north-south extension of the southern HTO, which is expressed by extrusion of the Greater Himalayan crystalline complex and formation of the Kailas basin and Konglong A-type magmatism. Meanwhile, intense ultrapotassic and leucogranitic magmatism began to occur within an extensional setting.

(3) The north-south extensional process likely ceased at ca. 18–17 Ma with a tectonic conversion to north-south contraction. This was marked by the development of the Main Boundary thrust, Main Frontier thrust, and widespread north-south–trending rifts in the Himalaya and Lhasa since 18 Ma (Williams et al., 2001). This transformation likely indicates that the orogen began to revert to a hard-collision mode with the Indian plate underthrusting northward beneath southern Tibet (DeCelles et al., 2011).

ACKNOWLEDGMENTS

We thank Dennis Brown, Bill White, and three anonymous reviewers for their constructive comments, which significantly improved our paper. Financial support was provided by the National Natural Science Foundation of China (91855215 and 41630208), Strategic Priority Research Program (A) of the Chinese Academy of Sciences (CAS; XDA2007030402), Key Program of the CAS (QYZDJ-SSW-DQC026), and the Guangzhou Institute of Geochemistry, CAS (GIGCAS 135 Project 135TP201601). This is contribution IS-2613 from GIGCAS.

REFERENCES CITED

Chen, J., Xu, J., Wang, B., Kang, Z., and Li, J., 2010, Origin of Cenozoic alkaline potassic volcanic rocks at KonglongXiang, Lhasa terrane, Tibetan Plateau: Products of partial melting of a mafic lower-crustal source?: Chemical Geology, v. 273, p. 286–299, https://doi.org/10.1016/j.chemgeo.2010.03.003.

Chen, M., Niu, F., Tromp, J., Lenardic, A., Lee, C., Cao, W., and Ribeiro, J., 2017, Lithospheric foundering and underthrusting imaged beneath Tibet: Nature Communications, v. 8, p. 15659, https://doi.org/10.1038/ncomms15659, erratum available at https://doi.org/10.1038/s41467-018-05925-8.

Chen, Y., Li, W., Yuan, X., Badal, J., and Teng, J., 2015, Tearing of the Indian lithospheric slab beneath southern Tibet revealed by SKS-wave splitting measurements: Earth and Planetary Science Letters, v. 413, p. 13–24, https://doi.org/10.1016/j.epsl.2014.12.041.

Chung, S., Chu, M., Zhang, Y., Xie, Y., Lo, C., Lee, T., Lan, C., Li, X., Zhang, Q., and Wang, Y., 2005, Tibetan tectonic evolution inferred from spatial and temporal variations in post-collisional magmatism: Earth-Science Reviews, v. 68, p. 173–196, https://doi.org/10.1016/j.earscirev.2004.05.001.

DeCelles, P., Robinson, D., and Zandt, G., 2002, Implications of shortening in the Himalayan fold-thrust belt for uplift of the Tibetan Plateau: Tectonics, v. 21, p. 12-1–12-25, https://doi.org/10.1029/2001TC001322.

DeCelles, P., Kapp, P., Quade, J., and Gehrels, G., 2011, The Oligocene–Miocene Kailas Basin, southwestern Tibet: Record of post-collisional upper plate extension in the Indus-Yarlung suture zone: Geological Society of America Bulletin, v. 123, p. 1337–1362, https://doi.org/10.1130/B30258.1.

Eby, G., 1992, Chemical subdivision of the A-type granitoids: Petrogenetic and tectonic implication: Geology, v. 20, p. 641–644, https://doi.org/10.1130/0091-7613(1992)020<0641:CSOTAT>2.3.CO;2.

Frost, B., Barnes, C., Collins, W., Arculus, R., Ellis, D., and Frost, C., 2001, A geochemical classification for granitic rocks: Journal of Petrology, v. 42, p. 2033–2048, https://doi.org/10.1093/petrology/42.11.2033.

Guo, Z.F., Wilson, M., Zhang, M., Cheng, Z., and Zhang, L., 2015, Post-collisional ultrapotassic mafic magmatism in South Tibet: Products of partial melting of pyroxenite in the mantle wedge induced by roll-back and delamination of the subducted Indian continental lithosphere slab: Journal of Petrology, v. 56, p. 1365–1406, https://doi.org/10.1093/petrology/egv040.

Hao, L.-L., Wang, Q., Wyman, D., Qi, Y., Ma, L., Huang, F., Zhang, L., Xia, X., and Ou, Q., 2018, First identification of mafic igneous enclaves in Miocene lavas of southern Tibet with implications for Indian continental subduction: Geophysical Research Letters, v. 45, p. 8205–8213, https://doi.org/10.1029/2018GL079061.

Hou, Z., Zheng, Y., Zeng, L., Gao, L., Huang, K., Li, W., Li, Q., Fu, Q., Liang, W., and Sun, Q., 2012, Eocene–Oligocene granitoids in southern Tibet: Constraints on crustal anatexis and tectonic evolution of the Himalayan orogeny: Earth and Planetary Science Letters, v. 349–350, p. 38–52, https://doi.org/10.1016/j.epsl.2012.06.030.

Rapp, R., Shimizu, N., and Norman, M., 2003, Growth of early continental crust by partial melting of eclogite: Nature, v. 425, p. 605–609, https://doi.org/10.1038/nature02031.

Wang, C., Dai, J., Zhao, X., Li, Y., Graham, S., He, D., Ran, B., and Meng, J., 2014, Outward-growth of the Tibetan Plateau during the Cenozoic: A review: Tectonophysics, v. 621, p. 1–43, https://doi.org/10.1016/j.tecto.2014.01.036.

Wang, Q., et al., 2016, Pliocene–Quaternary crustal melting in central and northern Tibet and insights into crustal flow: Nature Communications, v. 7, p. 11888, https://doi.org/10.1038/ncomms11888.

Wang, R., Weinberg, R., Collins, W., Richards, J., and Zhu, D., 2018, Origin of postcollisional magmas and formation of porphyry Cu deposits in southern Tibet: Earth-Science Reviews, v. 181, p. 122–143, https://doi.org/10.1016/j.earscirev.2018.02.019.

Whalen, J., Currie, K., and Chappell, B., 1987, A-type granites: Geochemical characteristics, discrimination and petrogenesis: Contributions to Mineralogy and Petrology, v. 95, p. 407–419, https://doi.org/10.1007/BF00402202.

Williams, H., Turner, S., Kelley, S., and Harris, N., 2001, Age and composition of dikes in southern Tibet: New constraints on the timing of east-west extension and its relationship to postcollisional volcanism: Geology, v. 29, p. 339–342, https://doi.org/10.1130/0091-7613(2001)029<0339:AACODI>2.0.CO;2.

Wu, F., Liu, Z., Liu, X., and Ji, W., 2015, Himalayan leucogranite: Petrogenesis and implications to orogenesis and plateau uplift: Acta Petrologica Sinica (Yanshi Xuebao), v. 31, p. 1–36.

Yin, A., and Harrison, T., 2000, Geologic evolution of the Himalayan-Tibetan orogeny: Annual Review of Earth and Planetary Sciences, v. 28, p. 211–280, https://doi.org/10.1146/annurev.earth.28.1.211.

Zhao, Z., et al., 2009, Geochemical and Sr-Nd-Pb-O isotopic compositions of the postcollisional ultrapotassic magmatism in SW Tibet: Petrogenesis and implications for India intra-continental subduction beneath southern Tibet: Lithos, v. 113, p. 190–212, https://doi.org/10.1016/j.lithos.2009.02.004.

Zheng, Y., Hou, Z., Fu, Q., Zhu, D., Liang, W., and Xu, P., 2016, Mantle inputs to Himalayan anatexis: Insights from petrogenesis of the Miocene Langkazi leucogranite and its dioritic enclaves: Lithos, v. 264, p. 125–140, https://doi.org/10.1016/j.lithos.2016.08.019.

Printed in USA